Materials Science & Engineering A 583 (2013) 129–139

Contents lists available at SciVerse ScienceDirect

Materials Science & Engineering A

journal homepage: www.elsevier.com/locate/msea

Stress induced martensitic transformations and phases stability in Cu–Al–Be shape-memory single crystals

F. de Castro Bubani [a,b], M. Sade [a,b,c,*], V. Torra [d], F. Lovey [a,c], A. Yawny [a,b,c]

[a] Centro Atómico Bariloche (CNEA), Av. E. Bustillo km. 9.5, (8400) S.C. de Bariloche, Argentina
[b] CONICET, Argentina, Av. Rivadavia 1917, (C1033AAJ) Buenos Aires, Argentina
[c] Instituto Balseiro, Universidad Nacional de Cuyo, Av. E. Bustillo km. 9.5, (8400) S.C. de Bariloche, Argentina
[d] Polytechnical University of Catalonia, C. Jordi Girona, 31, 08034 Barcelona, Spain

ARTICLE INFO

Article history:
Received 29 April 2013
Received in revised form
27 June 2013
Accepted 30 June 2013
Available online 5 July 2013

Keywords:
Shape-memory alloys
Mechanical characterization
Martensitic transformations
Phase transformation

ABSTRACT

The stress induced martensitic transformations between different metastable phases in Cu–Al–Be shape-memory alloy single crystals were assessed experimentally. In particular, the successive stress induced transformations from the high temperature austenitic DO_3 structure (β_1) to the 18R and to the 6R martensites were considered. Several distinct features which characterize the stress induced transformations in Cu–Al–Be and distinguish this system from other Cu-based shape-memory alloys are reported in this work. It was found that the 6R phase forms from a distorted 18R and that this stress induced transformation is highly reversible with no plastic deformation accompanying the process. The stress induced transformation from the distorted 18R to the 6R structure exhibits wide hysteresis, comparable with values observed in the NiTi system. A slightly negative temperature dependence of the critical stress to induce the 6R martensite was determined. Finally, a stress–temperature phase transformation diagram involving the metastable β_1, 18R and 6R phases is proposed.

1. Introduction

Ternary Cu-based (e.g., Cu–Zn–Al, Cu–Al–Ni, Cu–Al–Be) shape-memory alloys (SMAs) exhibit an interesting behavior related with the solid to solid transitions between different metastable phases [1–4]. They include the high temperature β_1-phase, usually referred to as austenite, and several low temperature phases, usually referred to as martensites. The most relevant structures are named 18R, 6R and 2H [1,5,6].

The high temperature austenitic phase is obtained from the sufficiently rapid cooling of a disordered bcc structure (A2). Different atomic ordering processes might take place during cooling, depending on the exact composition of the metallic system considered [7–9]. From now on, we will use austenite or β_1 to differentiate the ordered structure obtained after cooling from the disordered one stable at high temperatures. The β_1 phase and the martensitic structure which forms from it are metastable phases. The type of martensite which is thermally or stress induced from the β_1 austenite depends on the particular composition of the alloy being considered. As an example, in Cu–Zn–Al alloys with electron to atom concentration $e/a=1.48$, 18R martensite is formed. This martensite is characterized by a slightly monoclinic structure with a stacking period of 18 planes. Cu–Zn–Al alloys with higher e/a ratios show, instead, a transformation from β_1 into 2H martensite. The latter structure is described by an orthorhombic structure with a stacking sequence of 2 planes [2,5,6]. Both 18R and 2H martensites might also form in the Cu–Al–Ni system. In this case, the dependence of the type of martensite on the composition has been nicely shown by Recarte et al. [10], where higher Ni content is shown to favor the formation of 18R martensite.

Both 18R and 2H martensites may transform into other martensitic structures when stresses are applied. These martensite to martensite transitions are also diffusionless, solid to solid phase transformations, similar to the β_1 to martensite transition mentioned in the previous paragraph. An example of martensite to martensite transition has been reported by Otsuka et al. in Cu–Al–Ni alloys [4]. These authors have shown that further straining the 2H martensite formed from the austenitic structure results in a martensitic structure referred to as $18R_2$. This structure differs from the 18R martensite in the stacking of basal planes [11]. A similar transformation was reported by Arneodo et al. to occur in Cu–Zn–Al alloys with an electron concentration per atom $e/a=1.53$ [12]. In the context of the present work, an important transition is

* Corresponding author at: Centro Atómico Bariloche (CNEA), Av. E. Bustillo km. 9.5, (8400) S.C. de Bariloche, Argentina. Tel.: +54 294 4445265; fax: +54 294 4445290.
E-mail addresses: franco@cab.cnea.gov.ar (F. de Castro Bubani), sade@cab.cnea.gov.ar, marcossade05@yahoo.com.ar (M. Sade), vtorra_1@yahoo.com (V. Torra), lovey@cab.cnea.gov.ar (F. Lovey), yawny@cab.cnea.gov.ar (A. Yawny).

0921-5093/$ - see front matter © 2013 Elsevier B.V. All rights reserved.
http://dx.doi.org/10.1016/j.msea.2013.06.071

the one taking place between the 18R and the 6R martensites. This transformation can be stress induced by tensile deformation of a stress-induced 18R single crystal and it has been reported to occur in Cu–Zn–Al and Cu–Al–Ni alloys [3,4,13–15]. Two characteristics associated with this transition are worth being emphasized here. On the one hand, it has been reported that the critical stress to induce the 6R martensite shows a slight or even null dependence on temperature [1,3,14,16,17]. Additionally, the reported stress hysteresis associated to the 18R–6R transition is wider than the one involved in the β_1–18R transition. These parameters have been assessed in Cu–Al–Ni [18] and Cu–Zn–Al by several authors [15,19].

A noticeable and interesting result concerning mechanical properties of the 6R martensite in Cu–Zn–Al alloys has been reported by Cuniberti et al. [20]. These authors have shown that the critical stress to deform the 6R martensite plastically is smaller than the critical stress to induce the formation of the 6R structure. This leads to 6R plastic deformation concomitant with its own formation. This conclusion could also be inferred from previous reported results [15–17]. More recently, Bubani et al. [19] have shown that after introducing a homogeneous distribution of γ nano-precipitates in Cu–Zn–Al single crystals of electronic concentration 1.48, plastic deformation of the 6R phase can be shifted to a higher stress level. This allowed the authors to obtain the stress induced 6R martensitic structure without plastic deformation [19]. Thus, these systems are highly flexible as it is possible to use the β_1–18R (low hysteresis) and 18R–6R (high hysteresis) individually, or the combination of both, i.e., β_1–18R–6R (high strain), depending on prospective application requirements (actuator, damping devices, etc.).

Among the Cu-based shape-memory alloys, Cu–Al–Be alloys exhibit a distinct behavior concerning stress induced martensitic transitions. Several papers have shown that, after tensile stressing a β_1 single crystal, an 18R single crystal is formed [21–23]. More recently, it has been shown, however, that the β_1–18R transition exhibits an increase in mechanical hysteresis and associated deformation with test temperature. In addition, a deviation from linearity in the temperature dependence of critical transformation stresses to transform and retransform is observed [24]. These tendencies allow the behavior of Cu–Al–Be to be considered anomalous with respect to other Cu-based systems. The aforementioned peculiarities could be explained by the presence of a stress induced structural distortion of the 18R martensite in Cu–Al–Be alloys. Its occurrence has been experimentally determined in a wide temperature range. It was found that the distortion takes place in an extended stress range, resembling the stress induced R-phase transformation in NiTi shape-memory alloys [25]. This stress induced distortion of the 18R phase exhibits a positive dependence of the characteristic stresses on temperature (approximately a fifth the value of the β_1 to 18R transformation), no hysteresis and a maximum associated strain close to 1%. A change in the lattice cell parameters on the basal plane, similar to what has been reported for the 2H martensite in Cu–Zn–Al single crystals [12], was suggested to explain the distortion of the 18R structure [24]. Therefore, in the Cu–Al–Be system the 6R structure is stress induced from the distorted 18R phase to which we will refer as 18R′. Additionally, preliminary results have shown that high hysteresis is also present in Cu–Al–Be single crystals and no plastic deformation takes place during transformation.

Considering these attractive properties, the formation of 6R martensite might play an interesting role from the point of view of applications in damping devices. However, a deeper understanding is required to improve the comprehension of the mechanical properties associated to stress induced transitions in this ternary system considering the significant differences reported when compared with Cu–Al–Ni and Cu–Zn–Al alloys. This manuscript focuses on the assessment of the metastable phase transformation diagram of the Cu–Al–Be system. Single crystals are used for this purpose and stress induced transitions under tensile mode are analyzed in detail.

Table 1
Samples used in the present work and type of tests and measurements performed. A and B identify single crystals, the number that follows identifies different samples obtained with each crystal and used in the present manuscript. ER= electrical resistivity measurements (see critical transformation temperatures in the text).

Sample	ER	Temperature range of tensile tests (K)	Phase transition analyzed
A1	x		
B1	x		
A2		303–393	β_1–18R 18R–18R′ 18R′–6R
A3		303–393	β_1–18R 18R–18R′
A4		203–293	β_1–18R 18R–18R′
A5		243–353	β_1–18R 18R–18R′ 18R′–6R
B2		373	β_1–18R 18R–18R′ 18R′–6R

2. Experimental details

Two Cu–Al–Be single crystals with nominal composition Cu–11.4 wt% Al–0.53 wt% Be (Cu–22.63 at%Al, 3.15 at% Be) provided by Nimesis as wires 1.3 mm in diameter and 200 mm in total length were used for the present experiments. Crystals will be referred to as crystal A and crystal B. The orientation of the single crystal axes was determined by the X-Ray Laue method. It lies 7° from [001] towards [011] direction. Crystallographic Miller indexes will be referred to the austenitic β_1 structure unless specifically stated. Specimens with different lengths, 60 mm for mechanical testing and 10–20 mm for electrical resistivity measurements, were obtained from the single crystals by cutting with a low speed saw.

Specimens from crystal A were heat treated in the following way: 900 s (15 min) at 1110 K and quenched into water at 373 K. After 3600 s (60 min) at this temperature, samples were air cooled and then mechanically and electrolytically polished (7 steps, 9 V in a solution 15% of nitric acid in methanol). Crystal B samples were heat treated in this way: 600 s (10 min) at 1173 K, quenched in water at 303 K, kept at 373 K for 4 h and air cooled. Specimens were labeled by a number following the name of the crystal, i.e., specimen A1, etc. Both thermal treatments enable us to obtain the β_1 austenitic structure above room temperature and to reduce the concentration of vacancies [24].

The martensitic transformation temperatures for the heat treated condition were determined by electrical resistivity (ER) measurements by the four leads method. The following characteristic temperatures were obtained: M_s=296 K, M_f=246 K, A_s=270 K and A_f=302 K and M_s=314 K, M_f=220 K, A_s=268 K and A_f=318 K, for specimens A1 and B1, respectively (Table 1).

Mechanical tests were performed with an Instron 5567 electromechanical testing machine equipped with an Instron 3119-005 temperature chamber which allowed testing in the 203–523 K temperature range. 60-mm-long tensile specimens were cut from the original 200 mm crystals. A free length between grips of 40 mm was used. Deformation was measured with an MTS 632.13F-20 extensometer with a gage length of 10 mm attached to the central portion of the specimen. Tests were performed at a

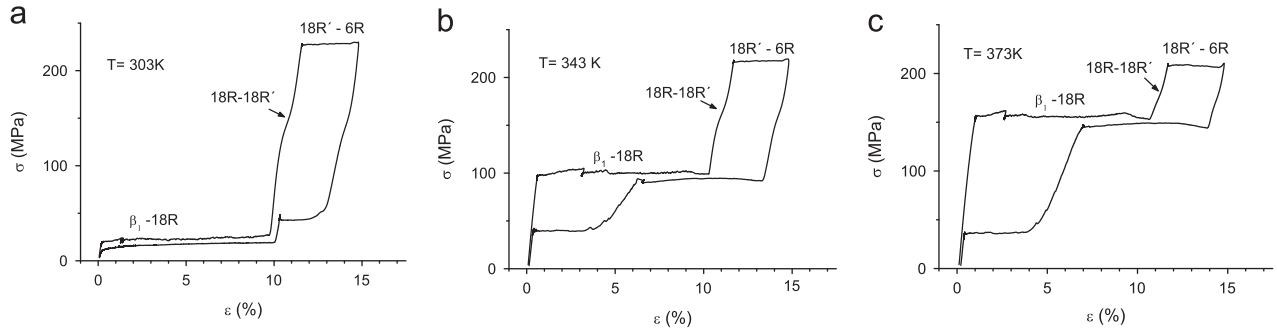

Fig. 1. $\sigma-\varepsilon$ curves obtained at different temperatures for sample A2 up to a partial formation of 6R. (a) $T=303$ K, (b) $T=343$ K and (c) $T=373$ K.

crosshead speed equal to or lower than 0.3 mm/min which has been shown to be adequate for avoiding temperature effects associated to the heat of transformation [19]. This corresponds to a mean strain rate of $1.25\times10^{-4}\,s^{-1}$ ($v=0.3$ mm/min, distance between grips=40 mm). Load was measured by an Instron 2525-810 Load Cell with ±1 kN maximum load.

Test temperatures were measured by a Chromel–Alumel thermocouple fixed to one of the grips, close to the griped zone of the specimen. The different specimens used in the tests reported in the present work are listed and specific test details are provided in Table 1.

A set of tests was performed at several temperatures to obtain the critical stress to transform to the 6R martensite. In order to do this, specimens in the β_1 structure were tensile stressed up to the stress necessary to obtain a small fraction of the 6R phase. These experiments allowed us to obtain the different critical applied stresses: i.e., the stress to induce the 18R structure, the stress to distort it according to previous results [24] and the stress to transform from the structurally distorted (18R′) structure to the 6R phase (18R′–6R transition). Critical stresses to retransform from 6R were also obtained. In addition, experiments where the amount of stress induced 6R martensite was progressively increased in consecutive cycles were also performed.

3. Experimental results

Fig. 1 illustrates the $\sigma-\varepsilon$ response at three different temperatures for the Cu–Al–Be material studied in the present work. Starting from the unloaded β_1 phase, the 18R martensite is first induced by increasing strain in the three situations represented. The first plateau level indicated as $\beta_1\rightarrow18R$ corresponds to this transition. By further increasing strain, the 6R martensite will be induced and a second distinct plateau denoted as $18R'\rightarrow6R$ arises. As seen in the figures, both plateau levels tend to overlap as the temperature is increased. This is due to the higher sensitivity to temperature exhibited by the critical stress for the $\beta_1\rightarrow18R$ transformation. In effect, previous results obtained by the present authors have shown that for the same material and composition, 393 K is the upper temperature to avoid overlapping between the successive stress induced forward transformations $\beta_1\rightarrow18R$ and $18R'\rightarrow6R$ [24].

In the three experiments shown in Fig. 1, only a fraction of the specimens was transformed to 6R martensite and this is the reason for the reduced plateau length of nearly 3% strain observed for this transformation. Between the two distinct plateaus mentioned before, the stress induced distortion of the 18R takes place. As seen on the three curves shown in Fig. 1, this transition occurs in an extended stress range giving the characteristic s-shaped feature denoted as 18R–18R′. The stress range associated with the 18R–18R′distortion exhibits a well-defined 0.4 MPa/K linear dependence on temperature as determined in [24]. This value is approximately a fifth the value of the slope corresponding to the β_1–18R structures. As a consequence, an increasing overlap between the β_1–18R transition and the 18R–18R′ distortion is noticed as temperature increases. This can be observed by comparing the $\sigma-\varepsilon$ curves obtained at 343 and 373 K shown in Fig. 1b and c, respectively. However, both the β_1–18R transformation and the 18R–18R′ distortion remain clearly below the critical stress to obtain 6R in the whole temperature range analyzed. As a consequence, the phase that might transform to 6R is actually the distorted 18R′ phase, not the 18R phase originally formed from the β structure.

The critical stresses to obtain the 6R martensite have been determined, as well as the stresses required to obtain 18R and to distort it. This has been done for several samples (see Table 1, samples A2, A3, A4 and A5 were used for this). Values for the critical stresses to obtain 18R from β_1 and to distort 18R into 18R′ were previously reported [24] for a smaller amount of samples. The new data, particularly the critical stresses to obtain the 6R structure, enable us to present the metastable σ–T phase transformation diagram of this system, to which the 18R–18R′ distortion adds an interesting difference compared to other Cu based systems. This will be done below since it is convenient to present additional results before discussing the phase transformation diagram.

Further analysis of the curves presented in Fig. 1 allows us to distinguish between two situations. In the first case, corresponding to the curve shown in Fig. 1a, the stress induced β_1-18R and 18R′–6R occur in sequential order i.e., forward and reverse paths of both β_1-18R and 18R′–6R transformations do not overlap (the transformation to 6R and retransformation to 18R take place at stresses above the ones corresponding to the β_1–18R stress induced cycle). Fig. 1a also allows us to appreciate the remarkable difference between the hysteresis associated with both stress induced transformations. Values of 5–10 MPa characterize the stress hysteresis for the β_1–18R transformation while values of 200 MPa are typical of the 18R–6R transition. In the second case, represented by the curve shown in Fig. 1b and c, the retransformation from 6R to the 18R takes place at a stress smaller than the one required to retransform from 18R to β_1 in case no 6R were induced. The alloy composition and crystal orientation of the specimens used favor the second type of behavior in the temperature range explored in the present work.

Fig. 2 shows several stress–strain curves obtained for sample B2 where the amount of 6R increases in each consecutive cycle at $T=323$ K. Fig. 2a shows two overlapping curves obtained before transforming to 6R, where the β_1–18R transition and the 18R–18R′ distortion are well observed. The overlap between the curves indicates that the material is in a well-defined reference state at the mentioned test temperature and the plotted curves give a reference start behavior concerning the β_1–18R–18R′ transitions.

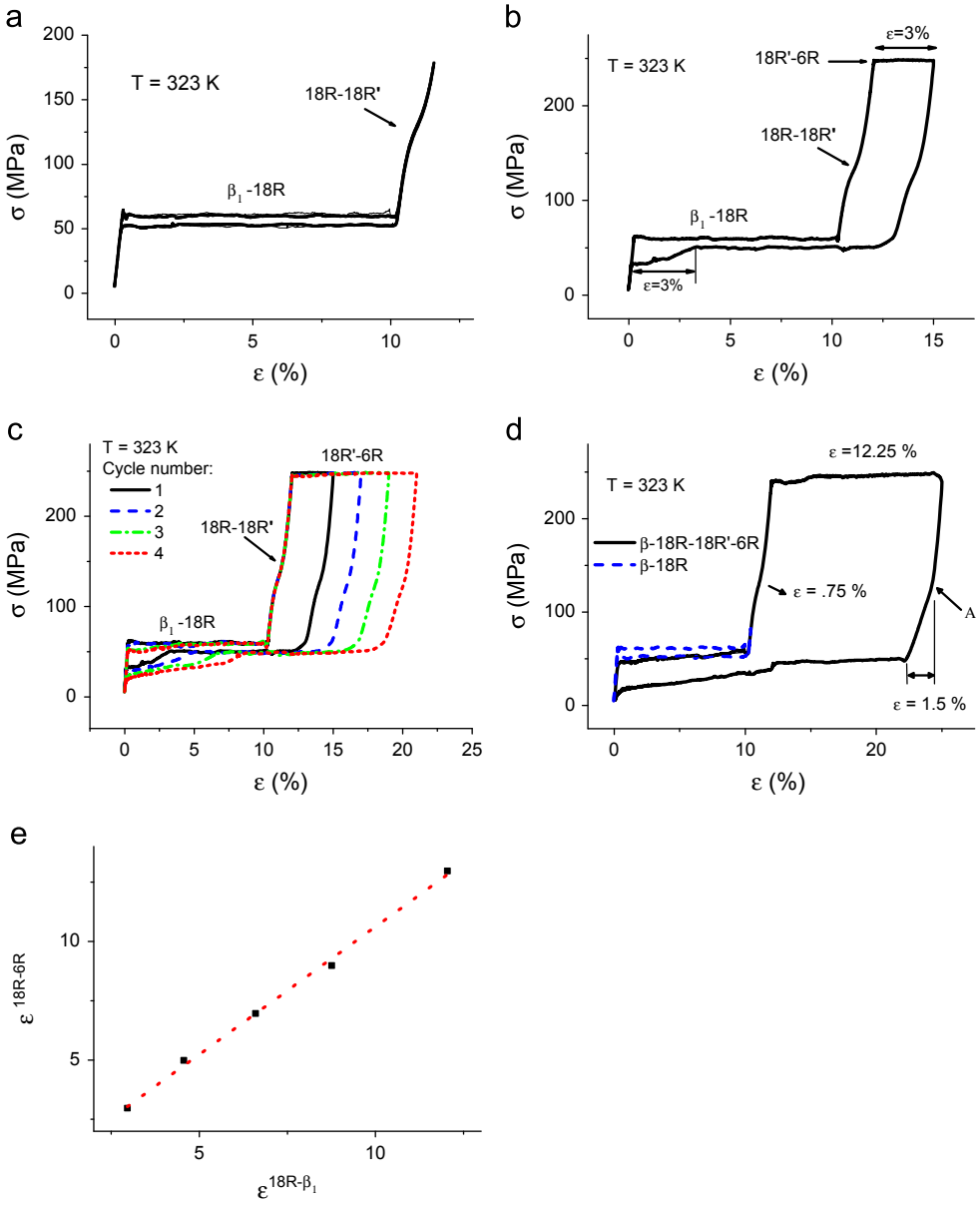

Fig. 2. Stress–strain curves obtained a $T=323$ K for sample B2. At the start condition $\sigma^{6R-18R}=\sigma^{18R-\beta_1}$. (a) 2 overlapping cycles including the β_1–18R and 18R–18R′ distortion, (b) a tensile cycle including partial transformation to 6R, (c) several cycles increasing the amount of 6R martensite formed and (d) final cycle leading to complete transformation to 6R. Initial $\sigma-\varepsilon$ cycle is also shown for comparison. Speed = 0.3 mm/min, (e) linear correlation between $\varepsilon^{18R'-6R}$ and $\varepsilon^{18R'-\beta_1}$.

Fig. 2b shows a transformation curve where a partial transformation to 6R is obtained at a well-defined stress. A deformation of 3% corresponds to the 18R′–6R transition. On unloading, the retransformation from 6R takes place at the same stress required to retransform 18R to β_1 (51 MPa). The observed plateau at this stress corresponds to the 18R–β_1 retransformation from the 18R not previously transformed to 6R and to the retransformation from 6R to 18R. Finally, the stress decreases to complete the 18R–β_1 retransformation corresponding to the portion of the sample which had previously transformed to 6R on loading the sample. A noticeable point here is the resultant stabilization of the 18R phase as referred to austenite, for the portion of 18R that had previously transformed to 6R. Transforming to 6R lowers the 18R–β_1 stress and this effect is also clearly observed in Fig. 2c where several stress–strain curves for different amounts of formed 6R are shown. In each case, the retransformation from 18R to β_1 takes place at smaller stresses for that part of the sample that had previously transformed to 6R, in comparison with the reference cycle of Fig. 2a. An interesting point to notice here is that the temperature used for tests shown in Fig. 2 can be considered a critical temperature which separates the different situations considered above: lower temperatures lead to β_1–18R and 18R′–6R cycles clearly separated from each other and higher temperatures lead to stresses to retransform from 6R to 18R smaller than the stress to retransform from 18R to β_1. The sequence of retransformation can be well assessed as the amount of material which transforms to 6R corresponds precisely to the amount of 18R which retransforms to β_1 at stresses smaller than the ones obtained at the reference condition shown in Fig. 2a. This has been verified by plotting $\varepsilon^{18R'-6R}$ vs. $\varepsilon^{\beta_1-18R}$. A linear correspondence between these values is obtained (Fig. 2e), which supports the retransformation sequence suggested.

From this experiment performed at a test temperature where the critical stresses to retransform from 6R to 18R and to retransform to the β_1 phase at the reference cycle are extremely close, several interesting features are to be noticed. On the one hand, no

remnant deformation was observed in any of the experiments. This implies that plastic deformation is absent in the whole deformation range considered. This is in variance with experimental results obtained with Cu–Zn–Al single crystals, where the formation of 6R usually shows concomitant plastic deformation of this phase, as mentioned above [20]. An interesting consequence of not having plastic deformation is that the distortion of the 18R phase found in Cu–Al–Be single crystals must disappear during retransformation in order to recover the β_1 phase. The morphology of the curves during the loading phase of the 18R structure is strictly the same, which is clearly understood as, in every case, the start point of each tensile curve corresponds to the β_1 single crystal and because the distortion takes place at a well-defined range of stresses that depends on test temperature, which is kept constant during consecutive cycles. At the test temperature used in Fig. 2, the 18R–18R′ distortion starts at a stress higher than the one required to have the whole sample as an 18R stress induced single crystal. This would not be the case for higher temperatures, as shown in a previous work (also see Fig. 1c) [24]. On the other hand, the morphology of the stress–strain curve during unloading from the 6R phase at stresses higher than the critical stress to retransform to 18R deserves some attention: it is very similar to the loading curve when the amount of 6R formed is small, but changes systematically as the amount of 6R martensite increases, up to 100% transformation. This can be understood considering that, at smaller amounts of formed 6R, the morphology of the retransformation curve is mainly determined by the 18R′–18R transition of the part of the sample that did not transform to 6R. If the whole sample transforms to 6R, the unloading curve in the stress region between $\sigma^{18R'-6R}$ and σ^{6R-18R} shows a linear behavior with a change in slope at a well-defined stress, i.e. 136 MPa (point A in Fig. 2d). This will be analyzed in the discussion section and will be related to a structural change in the opposite direction of the one reported for the 18R–18R′ distortion. The last point to consider here is the slope of the curve during retransformation from 18R to the β_1 phase. All curves, including some not plotted here for the sake of clarity, show that the stress to retransform from 18R to β_1 decreases for the part of the sample that previously transformed to 6R. This is well observed in Fig. 2b and also in 2c, where the deformation range of the inclined 18R–β_1 curve is nearly the same as the deformation corresponding to the 18R′–6R transition. This is also observed for larger fractions of formed 6R and, particularly, the last cycle obtained at 323 K shows a slope during both the transformation and retransformation between β_1 and 18R, with a larger hysteresis if compared with the reference cycle (see Fig. 2d, where the initial β_1–18R cycle is also plotted for comparison). This outcome seems to be the consequence of a stabilization effect enhanced by the transformation to the 6R phase. This point will be further analyzed in the discussion section. A following tensile test at a higher temperature (353 K) shows a clear decrease in the slope of the curves during the β_1–18R transformation (see Fig. 3). In the stress–strain curve shown in this figure, the amount of 6R formed is slightly smaller than the maximum attainable and, due to this, a small fraction of the sample retransforms from 18R to β_1 at approx. 101 MPa, i.e., at the critical value for the 18R –β_1 retransformation when no transformation to 6R has taken place. Most of the sample transformed to 6R and then retransformed to 18R and to β_1 at $\sigma = 40$ MPa, i.e. the critical stress to retransform from 6R to 18R also affects the stress to retransform to β_1. This fact can also be described as an 18R stabilization undoubtedly determined by retransformation from the 6R structure.

Additional experiments at temperatures lower than Ms have been performed and strongly suggest the formation of a 2H martensite. These results are being explored and will be presented in due course.

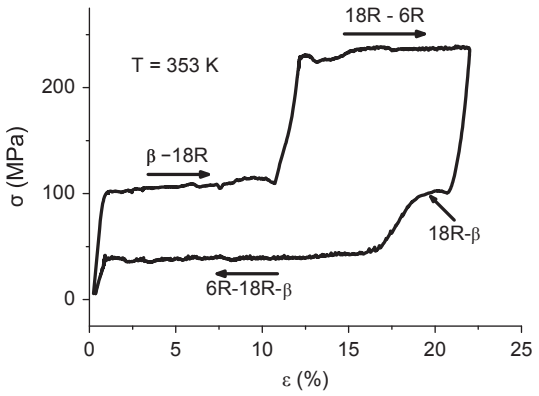

Fig. 3. Stress–strain curve for a cycle obtained at $T = 353$ K. Sample B2 is used. Partial transformation to 6R is performed. Two well defined stress plateaus are observed during retransformation: one at the higher stress for that part of the sample which did not transform to 6R, and the other which corresponds to the lower retransformation stress, for the portion of the sample previously transformed to 6R.

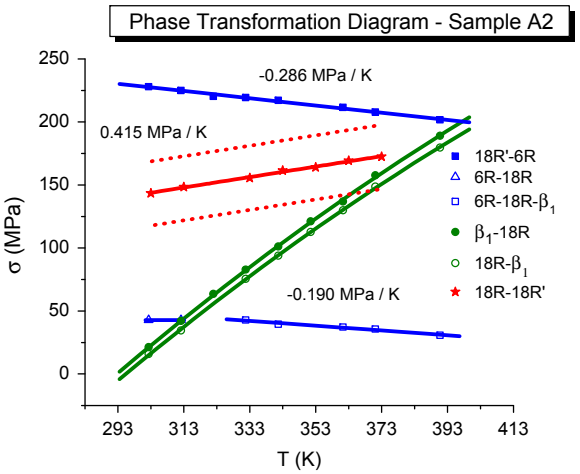

Fig. 4. Metastable stress–temperature phase transformation diagram for sample A2. Dotted lines indicate the stress range in which the 18R–18R′ distortion takes place.

From the experiments performed, the critical stresses for the transformations involved were obtained and plotted in a σ–T phase transformation diagram. Fig. 4 shows data obtained for sample A2. The temperature interval considered ranges from T close to A_f to the maximum temperature at which the β_1–18R and 18R′–6R transformations do not overlap. This is the temperature range for the largest possible pseudoelastic deformation, considering β_1 as the start point and a complete 6R stress induced crystal as the final condition. Some considerations are made here regarding these metastable phase transformation diagrams. On one hand, $\sigma^{\beta_1}-18R$, $\sigma^{18R-\beta_1}$, and $\sigma^{18R-18R'}$ critical stresses have been partially reported [24]. It has been shown that the distortion of the 18R structure does not present a stress plateau. Instead of this, the stress increases continuously within a well-defined stress range. Another difference between this distortion and the martensitic β_1–18R and 18R′–6R transitions is that no measurable hysteresis is associated to the 18R–18R′ distortion. In order to insert these data in the phase transformation diagrams of Fig. 4, the inflection point of the stress–strain curve during the 18R–18R′ transition was determined and the critical stress obtained was plotted to identify this structural change. Additionally, the stresses to start and end this transition are also shown in the figure. A linear fit of the inflection points determined as a function of test temperature gives a slope equal to 0.415 MPa/K for this sample. Slightly different values have

been obtained for other samples (0.417 MPa/K, 0.384 MPa/K, 0.373 MPa/K for samples A3, A4 and A5 respectively). However, this variation is not substantial considering that the 18R–18R′ distortion takes place in a stress range, does not show a stress plateau and that the inflection point of the $\sigma-\varepsilon$ curve has been selected as a reference point to determine its variation with temperature. From the stresses to obtain 6R, a linear fit with an excellent correlation can be obtained, giving a $d\sigma^{18R'-6R}/dT$ slope equal to -0.286 MPa/K (sample A2 in Table 1).There is no doubt concerning the sign of the stress–temperature dependence and the small effect that temperature has on the critical stress to obtain 6R. A linear dependence is also found for the variation of σ^{6R-18R}, albeit with a linear slope slightly smaller than the one obtained for the direct transformation.

4. Discussion

4.1. On the quasi-reversibility of the martensitic transformations

Several experimental results have been presented in the current paper in order to clarify the mechanical behavior associated to tensile stress induced phase transitions in Cu–Al–Be single crystals at temperatures higher than A_f. Particularly, the formation of the 6R structure has been considered and the critical stresses to obtain this structure have been determined in a wide temperature range, from A_f up to the highest temperature which does not show overlap between both martensitic transitions. Considering the formation of the 6R structure, several matters are to be analyzed. The first fact to be emphasized concerns the reversibility shown by the mechanical pseudoelastic cycle which involves both transitions, i.e. the β_1–18R and the formation of the 6R structure. In fact, we have shown that no permanent deformation is detected after retransformation to the austenitic structure. It is interesting to compare this behavior with the one found in Cu–Zn–Al alloys. In the latter system, reported data indicate that the critical stress to deform the 6R structure plastically lies below the applied stress required to obtain the 6R martensite, leading to plastic deformation at the same stress at which this martensite is formed [20]. One of the potential uses of the high hysteresis involved in the formation of 6R martensite is the dissipation of energy during oscillating events like earthquakes. Retained deformation, either by real plasticity of one or several of the involved structures or by stabilizing martensite, will decrease the amount of energy absorbed if several cycles are performed, which is an undesired effect [15,26]. A first approach to solve this problem in Cu–Zn–Al single crystals has been recently presented and considers the introduction of γ nanoprecipitates in the austenitic matrix [19]. These precipitates increase the required critical stress to deform the 6R martensite plastically, clearly separating the formation of this martensite from its plastic deformation. In fact, it has been possible to observe the elastic behavior and subsequent plastic deformation of the 6R structure after the introduction of 20 nm cubic precipitates [19]. Previous reported results on Cu–Al–Be single crystals have also shown that sequential transformations involving formation of 6R at $T>A_f$ do not lead to permanent plastic deformation [27,28]. If complete shape reversibility is required, Cu–Al–Be single crystals have an interesting advantage when compared with Cu–Zn–Al single crystals, due to the higher mechanical strength of the corresponding 6R martensite. Plastic properties of this structure are still to be studied and further experiments are required to determine the stabilization phenomenon properties of this martensite in order to evaluate the stability of the 18R–6R under cyclic requirements. This study is being performed at present. However, results presented in this manuscript are encouraging due to the mechanical reversibility after a tensile deformation higher than 20%. Additionally, reported results on the formation of 6R martensite in Cu–Al–Ni alloys also show stress–strain curves where no permanent deformation is retained [4]. However, the brittleness of this system is still a disadvantage when applications are considered [29].

4.2. On the crystallography of the martensitic transitions

4.2.1. The β_1–18R–18R′ distortion

The transformation into a 6R martensite has also been reported in Cu–Zn–Al and Cu–Al–Ni systems under similar thermodynamic requirements, i.e. tensile stressing the austenitic single crystal at a well-defined range of tensile axes (not far from [100]). However, an interesting situation must be considered when Cu–Al–Be single crystals are analyzed. The particular behavior arises if the mechanical behavior of the 18R single crystal is considered. For electronic concentration = 1.48, the 3 metallic systems mentioned show the austenite–18R stress induced martensitic transition at $T>A_f$. If the 18R martensite obtained is further tensile stressed, different results have been reported. As an example, in Cu–Zn–Al single crystals, the 18R martensite transforms to 6R martensite for tensile axes closer than 24° to [100] and shows brittle fracture if the tensile axis diverges from this orientation range. After fracture, 2H martensite has been found in the material, with no indication of its formation in the stress–strain curve [30]. Cu–Al–Ni alloys also show a direct 18R–6R transformation if a tensile load is applied to a tensile induced 18R single crystal if the tensile axis is the required one [31]. Instead of that, Cu–Al–Be single crystals present a distortion of the 18R single crystal if it is tensile stressed, which implies that the 6R structure forms from this distorted structure (named 18R′ here) instead of forming directly from the 18R structure. This distortion, which has been presented for the first time in reference [24], occurs in a stress range that shows a slight positive temperature dependence (approximately 0.4 MPa/K), not at a stress plateau like most of the stress induced martensitic transformations in Cu based alloys. Moreover, the single crystal deforms as the distortion takes place, the measured deformation being close to 1%. Examples of this distortion and the concomitant deformation are well observed in several figures (see, for example, Fig. 1a) at stresses lower than the one required to induce the 6R phase.

A strain similar to the one observed in the 18R martensite due to the 18R–18R′ distortion has been reported to take place in 2H martensite in Cu–Zn–Al alloys subjected to applied stresses [12]. The strain in the 2H martensite, close to 0.8%, was attributed to changes in the lattice parameters, possibly due to a second order phase transition. The same procedure was performed to analyze the 18R–18R′distortion in Cu–Al–Be single crystals [24], leading to results of the same order of magnitude. In the present work, the 18R′–6R transformation is studied in detail. The experimental results have shown that not only does the 18R–18R′ transformation take place in the 18R phase, but other changes are observed along the 18R–6R transformation cycle that may be related to crystallographic changes.

In order to have a self-consistent evaluation of the crystallography involved along the β_1–18R–18R′–6R -transformation cycle, we shall reconsider the analysis performed in the previous paper [24] concerning the 18R–18R′ transformation. In the present manuscript, in addition to the changes in the lattice parameters, the changes in the lattice invariant shear will be taken into account, whenever applicable. Lovey [32] noticed that when the lattice parameters change, modifying the deformation ψ of the basal planes, the magnitude of the vector which produces the lattice invariant shear also becomes dependent on ψ.

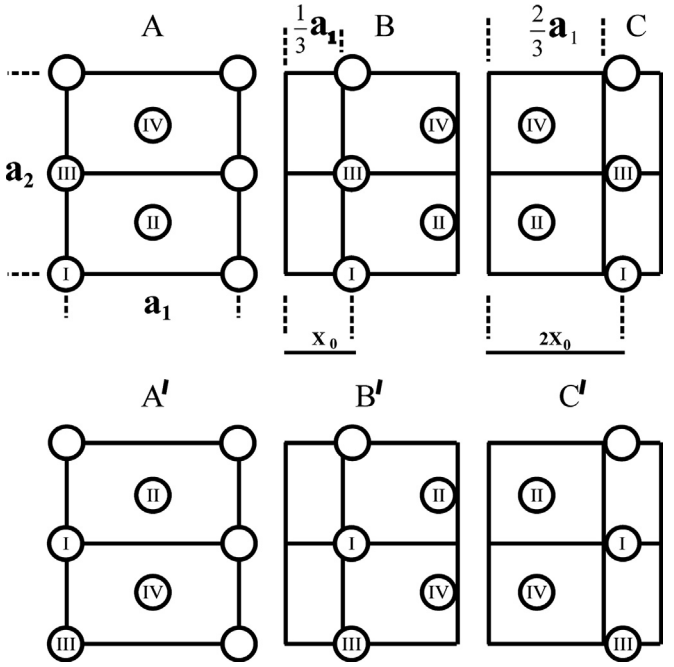

Fig. 5. Lattice sites at the possible basal planes in Cu–Al–Be close packed martensites. Planes B and C are formed from plane A by displacing all atoms in this plane a distance x_0 and $2x_0$ to the right, respectively. Planes A', B' and C' are obtained from the corresponding A, B and C planes after a displacement of $\pm(1/2)a_2$ (up or downwards). The distance x_0 depends on ψ.

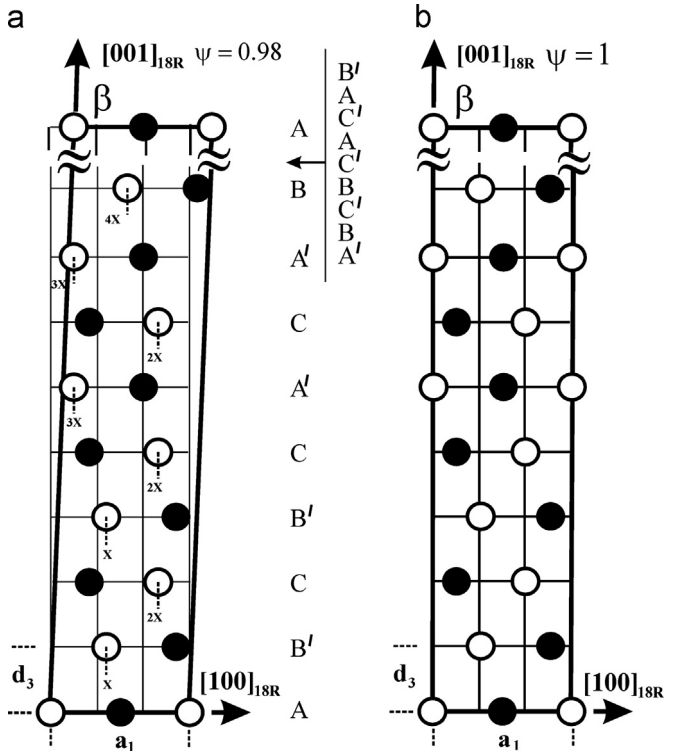

Fig. 6. (a) Modified 18R structure ($\psi = 0.98$, $\tan(\pi-\beta) = (\sqrt{2}/9((1-\psi^2)/\psi\ ))$ and $\beta = 89.6^\circ$). (b) Normal 18R structure ($\psi = 1$ and $\beta = 90^\circ$).

For clarity, we shall reproduce the atom arrangements at the basal planes of the closed packed martensites in Cu–Al–Be alloys, as in Fig. 5.

In Fig. 5, sites I, II and III are occupied by Cu in equal proportion. Site IV is occupied by Al and Be, up to 100% occupation for this site. The remaining Be is homogeneously distributed among sites I, II and III as to complete, together with Cu, 100% occupation in each site.

In Fig. 5, a_1 and a_2 are the lattice parameters along the $[100]_{18R}$ and $[010]_{18R}$ directions in the basal plane, respectively. Their values were obtained in [24] as

$$a_1 = (0.456 \pm 0.001)\ \text{nm}$$
$$a_2 = (0.534 \pm 0.001)\ \text{nm} \quad (1)$$

The lattice parameters of the 18R martensite can be expressed in terms of ψ and a_f [32], where a_f is the lattice parameter of the hypothetical FCT structure that can be formed with the basal planes in Fig. 5. Since the volume is conserved during the transformation from the β_1 phase to the 18R martensite to a good approximation [32], $a_f = a_\beta(2/\psi)^{1/3}$, where a_β is the lattice parameter of the fundamental BCC structure of the parent phase (disregarding the ordering).

Namely:

$$a_1 = \frac{a_f}{\sqrt{2}}\sqrt{(1+2\psi^2)} \quad (2)$$

$$a_2 = \frac{2a_f}{\sqrt{2}} \quad (3)$$

$$d_3 = \frac{a_f\psi}{\sqrt{(1+2\psi^2)}} \quad (4)$$

where d_3 is the interplanar distance normal to the basal planes. From (1), (2) and (3), the value of a_f, for this particular case, can be obtained ($a_f = (0.377 \pm 0.001)$ nm).

The deformation ψ of the basal planes is defined as

$$\psi = \sqrt{\frac{1}{2}\left[\left(\frac{2a_1}{a_2}\right)^2 - 1\right]} \quad (5)$$

Using (1) in (5) we obtain

$$\psi = 0.98 \pm 0.006 \quad (6)$$

The value of x_0 in Fig. 5 can be obtained from [32], as

$$x_0 = \frac{1}{3}a_1 + x \quad (7)$$

Where

$$x = \frac{\sqrt{2}}{3}a_f\frac{(1-\psi^2)}{\sqrt{1+2\psi^2}} \quad (8)$$

The 18R martensite is obtained by piling up the close packed basal planes, given in Fig. 5, following, for example, the sequence: $AB'CB'CA'CA'BA'BC'BC'AC'AB'A$. The 18R structures for $\psi = 0.98$ and $\psi = 1$ are shown in Fig. 6(a) and (b) respectively. In Cu–Zn–Al alloys, while the value of the deformation of the basal plane can attain a value up to $\psi = 1.02$ in 2H martensite [12], the 6R martensite seems to be more stable with $\psi = 1$ [33]. Since we are dealing with the 18R′–6R transformation in the Cu–Al–Be system, we shall restrict ourselves to a maximum value of $\psi = 1$.

In order to compute the difference in elongation between the 18R and 18R′ martensites in a more precise approach (compared with our previous work [24]), we shall consider the work of De Vos et al. [34]. It should be noted that the 9R and 18R martensites only differ in the atomic ordering, which is unimportant for the crystallographic theory. These authors give the shear strain S of the BCC – 9R transformation as a function of ψ for a small volume change ($\Delta V = 0.02\%$). By interpolation we obtained:

$$S_{\beta-18R}^{\psi=0.98} = 0.218 \pm 0.004 \quad (9)$$

and

$$S^{\psi=1}_{\beta-18R}=0.232 \tag{10}$$

It should be remarked that when the β_1 phase transforms into the 18R structure, a certain amount of faults are created by the lattice invariant shear in order to obtain an undistorted habit plane, the amount of faults depending on the deformation ψ. These random faults are not drawn in Fig. 6.

For example, let us take Fig. 6, the shear of the transformation from β to 18R with $\psi=0.98$ and $\psi=1$ is given by (9) and (10), respectively. When these two structures are built during the transformation, they will show different amounts of extra random basal plane stacking faults at the end, and a slightly different orientation of the habit plane. Therefore, changing the lattice parameters at this stage, for example, going from $\psi=0.98$ to $\psi=1$, will not produce the shear deformation given in (10), and vice versa; because the random extra faults will remain in the structures. However, the difference in the amount of extra stacking faults is very small [32], and we can take, to a good approximation, the value of the shear given in (10) to calculate the elongation of the 18R′ martensite ($\psi=1$) with reference to the 18R martensite ($\psi=0.98$), by taking the difference between (9) and (10).

The elongation strain of the transformation is defined as

$$\varepsilon_{tr}=\frac{(\ell-\ell_0)}{\ell_0} \tag{11}$$

Where ℓ_0 and ℓ are the length of the specimen before and after the transformation.

Following reference [35], the ideal elongation strain can be calculated as

$$\varepsilon_{tr}=\frac{S_{tr}\cos\varphi_0+\cos\lambda_0}{\cos\lambda}-1 \tag{12}$$

$$\varepsilon_{tr}=\frac{sen\lambda_0}{sen\lambda}-1 \tag{13}$$

Where $\varphi_0$and λ_0 are the angles between the tensile axis and the normal of the glide plane and the shear direction, respectively. S_{tr} is the transformation strain, like those in (9) and (10).

In the present case:

$$\varphi_0=42^\circ \text{ and } \lambda_0=48.6^\circ \tag{14}$$

The set of Eqs. (12) and (13) give the elongation strain ε_{tr} and the new angle λ as solutions, as the shear direction rotates towards the tensile axis.

From Table 2 we obtain

$$\Delta\varepsilon_{18R-18R'}=\varepsilon^{\psi=1}_{\beta_1-18R}-\varepsilon^{\psi=0.98}_{\beta_1-18R}=(7\pm2)\times10^{-3} \tag{15}$$

This value is in good agreement with the experimental value reported in [24] and found in sample B2 of Table 1. The elongation of the specimen upon transformation from β_1–18R for $\psi=0.98$ is 0.114 ± 0.002, a little longer that the measured experimental result in Fig. 2d, where 0.100 ± 0.001 is obtained. The slight difference between the experimental and calculated values can be rationalized considering the constraints imposed by the grips to the sample while the calculation considered that the tensile axis is free to rotate toward the shear direction.

4.2.2. The 18R′–6R transformation

Let us consider now the 18R′–6R transformation. We shall assume that the 18R′ martensite at the beginning of the 6R transformation comprises the full deformation of the basal plane $\psi=1$, and that the 6R phase inherits this basal plane configuration. The vector of the transformation is schematized in Fig. 7a.

Table 2
Elongation strain, $\varepsilon^{\psi}_{\beta_1-18R}$, and the correspondent angle, $\lambda^{\psi}_{\beta_1-18R}$, between shear direction and tensile axis, from Eqs. (12) and (13) as a function of ψ.

ψ	$S^{\psi}_{\beta_1-18R}$	$\varepsilon^{\psi}_{\beta_1-18R}$	$\lambda^{\psi}_{\beta_1-18R}$
0.98	0.218 ± 0.004	0.114 ± 0.002	42°
1	0.232	0.121	41.8°

The magnitude of the translation shear vector is

$$\mathbf{t}^{\psi=1}_{18R'-6R}=\frac{1}{3}\mathbf{a}_1 \tag{16}$$

In Fig. 7a. the angle $\gamma=90^\circ$. The corresponding shear deformation can be obtained from (2) and (4), for $\psi=1$, as

$$S^{\psi=1}_{18R'-6R}=\frac{1/3a_1}{3d_c}=\frac{\sqrt{2}}{6} \tag{17}$$

Using (17) in the set of Eqs. (12) and (13), with $\varphi_0=52^\circ$ and $\lambda_0=36^\circ$, we obtain:

$$\varepsilon^{\psi=1}_{18R'-6R}=0.121 \text{ and } \lambda^{\psi=1}_{18R'-6R}=31.6^\circ \tag{18}$$

This deformation is slightly greater than the experimental value obtained in the present manuscript (0.112 ± 0.002 for sample B2 in Fig. 2d) and the slight difference can be understood if the constraints imposed by the grips are considered.

4.2.3. The 6R–18R retransformation

On unloading, after having completed the 18R′–6R transformation in Fig. 2d, a change in slope at a stress of about 130 MPa is clearly noticed in the stress–strain curve, and a shortening of the specimen, which is larger than the correspondent elastic unloading of the 6R structure, takes place. When the retransformation to the 18R phase starts, at about 27 MPa, the total shortening of the specimen attains about 1.5% (with respect to the original ℓ_0 of the 18R phase).

In order to explain this shortening we assume that the changes in the lattice parameters from $\psi=0.98$ to $\psi=1$ that took place on loading the 18R structure (in the transformation from 18R to 18R′), reverse now from $\psi=1$ to $\psi=0.98$ on unloading the 6R phase from 130 MPa to 27 MPa. (This is shown in Fig. 7b). This hypothesis is reasonable since the change in slope of the $\sigma-\varepsilon$ curve takes place at a stress very close to the value obtained during the 18R–18R′ distortion and, additionally, both 18R and 6R martensites share the same basal plane. We have two contributions for this shortening. On one hand, the change in the lattice parameters will produce a change in the shear transformation vector and, on the other hand, the change in the lattice parameter itself will contribute to the shortening. Let us consider first the changes in the shear of the transformation.

The shear transformation vector is now

$$\mathbf{t}^{\psi<1}_{\mathbf{18R-6R}}=1/3\mathbf{a_1}-2\mathbf{x} \tag{19}$$

Where $\mathbf{a}_1$ and x were given in (2) and (8) respectively.

From (2), (4) and (8), the shear of the transformation becomes

$$S^{\psi<1}_{18R-6R}=\frac{t^{\psi<1}_{18R-6R}}{3d_c}=\frac{\sqrt{2}}{6}\frac{(2\psi^2-1)}{\psi} \tag{20}$$

The angles between the shear direction, the $\mathbf{a}_2$ direction and the normal of the basal plane, with the tensile axis, respectively, are:

$$\lambda_0=36^\circ, \text{and } \chi_0=89.9^\circ \text{ and } \varphi_0=52^\circ \tag{21}$$

We use the set of Eqs. (12) and (13) to obtain the solution for the elongation strain ε_{tr} and the new angle λ, as the shear direction

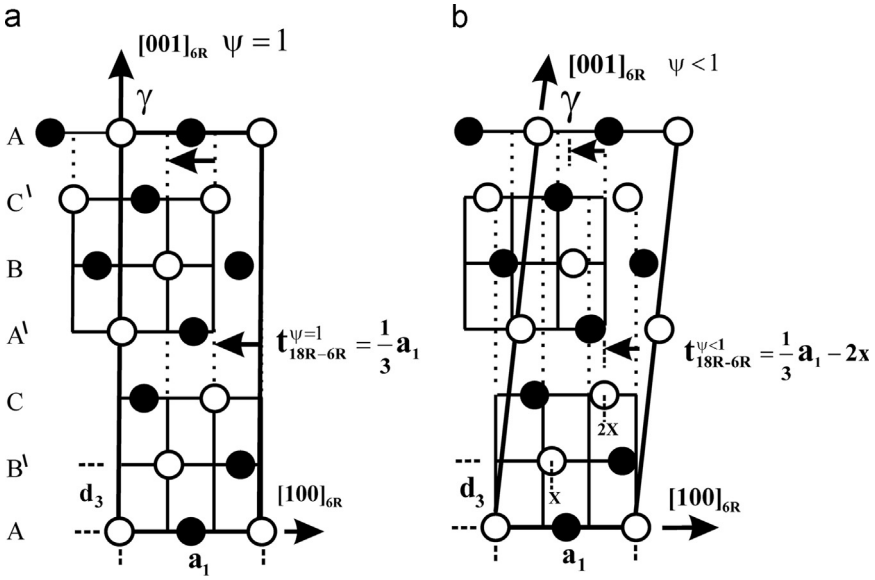

Fig. 7. The 6R structure is obtained from the 18R′ structure by applying the indicated shear vector once to the left every third basal plane. (a) corresponds to $\psi = 1$ while (b) corresponds to $\psi < 1$.

rotates towards the tensile axis. We obtain:

$$\varepsilon^{\psi=0.98}_{18R-6R} = 0.114 \text{ and } \lambda^{\psi=0.98}_{18R-6R} = 32^{\circ} \tag{22}$$

Using (18) and (21) we obtain the shortening of the specimen due to the accommodation of the shear translation vector given in (19). The specimen will shorten by

$$\Delta\varepsilon^{6R}_{Shear\ def} = \varepsilon^{\psi=0.98}_{18R-6R} - \varepsilon^{\psi=1}_{18R-6R} = -7 \times 10^{3} \tag{23}$$

Concerning the effect of the lattice parameters, we follow the work of Arneodo et al. [12]. These authors have shown that the elongation strain due to the change in lattice parameters in the martensite can be calculated as follows:

$$\varepsilon_j = \frac{a_j(\psi_f) - a_j(\psi_i)}{a_j(\psi_i)} \tag{24}$$

In terms of the lattice parameters given in (2) to (4) and where ψ_i and ψ_f are the initial and final values of the orthorhombic distortion, respectively.

When the martensite changes from having $\psi = 1$ to $\psi = 0.98$, the values of the strains defined in (24) are as follows:

$$\varepsilon_{a_1} = -6.62 \times 10^{-3}, \varepsilon_{a_2} = 6.75 \times 10^{-3}, \varepsilon_{a_3} = -0.09 \times 10^{-3} \tag{25}$$

The shortening of the specimen, $\Delta\varepsilon^{6R}_{Lattice}$, due to the changes of the lattice parameters, when ψ changes from ψ_i to ψ_f is given by [12]:

$$\varepsilon^{6R}_{Lattice} = \varepsilon_{a_1}\cos^2\lambda_0 + \varepsilon_{a_2}\cos^2\chi_0 + \varepsilon_{a_3}\cos^2\varphi_0 \tag{26}$$

Where λ_0, χ_0 and φ_0 are the angles given in (21).

Thus, using (21) and (25) in (26), we obtain, for the relative specimen shortening:

$$\Delta\varepsilon^{6R}_{Lattice} = -5.4 \times 10^{-3} \tag{27}$$

The total shortening when the 6R phase is unloaded from about 130 MPa to about 27 MPa is:

$$\Delta\varepsilon^{6R}_{Totalshort} = \Delta\varepsilon^{6R}_{Sheardef} + \Delta\varepsilon^{6R}_{Lattice} = -12.4 \times 10^{-3} \tag{28}$$

Which is very close to the elongation observed experimentally (see Fig. 2d).

The 6R phase with $\psi = 0.98$ retransforms to the 18R martensite also with $\psi = 0.98$.

4.2.4. Morphology of the $\sigma - \varepsilon$ curves

Several points are to be mentioned here. On one hand, two different mechanical behaviors can be clearly distinguished: (a) the whole 18R–6R–18R cycle takes place at stresses greater than the β_1–18R cycle and (b) the critical stress to retransform to 18R from 6R lies below the critical stress to retransform to the austenitic structure. For the composition used, test temperature will determine the shape of the curves obtained. As mentioned above, most of the stress strain curves obtained show no remnant deformation, which indicates better mechanical properties of the phases involved if compared with Cu–Zn–Al single crystals, at least if no precipitates are added to the latter system [19]. Additionally, the $\sigma - \varepsilon$ curves are different from those obtained in Cu–Zn–Al and Cu–Al–Ni alloys due to the presence of the 18R–18R′ distortion. This is clearly observed if the critical stress to obtain 18R is small enough. In case the temperature is increased, an overlap between the β_1–18R and the 18R–18R′ transitions is obtained, leading to larger deformation and wider pseudoelastic hysteresis. This has already been reported [24].

An interesting result has been presented in Fig. 2. The test temperature of the corresponding experiment is the critical one which separates both behaviors mentioned above. Temperatures lower than this one will show well separated tensile transformation cycles (Fig. 1a), while higher temperatures will lead to more complicated behavior during the retransformation stage (Fig. 1b and c). The curves obtained show that the 18R which retransformed from the 6R structure is in a stabilized condition. This case deserves some attention, considering the relevance of martensite stabilization in Cu based alloys. Although we do not intend to discuss this point in detail here, we shall mention that the effect of 6R stabilization has been analyzed in several papers on Cu–Zn–Al single crystals, whereas no information is available regarding Cu–Al–Be [33,36]. Additionally, it has been reported that, in Cu–Zn–Al alloys, 6R stabilization is favored if compared with stabilization in the 18R martensite since additional planes are available for the interchange of the atoms responsible for the stabilization in this system, according to reported results [26]. At the moment, there is no agreement on the literature as to the origin of 18R stabilization in Cu–Al–Be, although several papers have reported the existence of normal and hyper stabilization of this martensite, mainly in conditions where a large concentration of vacancies is present [37]. In the present paper, the amount of vacancies is

expected to be close to equilibrium and, in fact, 18R stabilization is rather small under quasistatic experiments, according to results not presented here. A different situation arises if dynamic tests are performed; in this case, the 18R martensite undergoes significant stabilization, at least one order of magnitude greater than quasistatic stabilization, at the same test temperature [38]. The results shown in Fig. 2 indicate a smaller retransformation stress from 18R to β_1 for that part of the material previously transformed to 6R martensite. This might be explained by the interaction between the retransformation front and 6R bands. However, this stabilization effect is not homogeneous, which might indicate a contribution of some diffusive phenomenon that triggers higher stabilization according to the time interval each part of the sample remains in 6R martensite. At the moment, the most plausible cause of this stabilization effect seems to be a mixture of pinning effects and diffusion. However, more data is required to understand this behavior and to propose an atomic mechanism to explain the stabilization of both martensites in this system.

Another interesting phenomenon that deserves our attention can be observed in Fig. 2. It is shown in Fig. 2c and d that, after the transformation to 6R martensite, not only does $\sigma^{18R-\beta_1}$ decrease, as mentioned above, but also a decrease in σ^{β_1-18R} is clearly observed in the following cycle. Although this point is not the main focus of the present manuscript, it is interesting to draw attention to the slow recovery of the austenitc structure formed from the stabilized 18R. In fact, the pseudoelastic slope is the same during the β_1–18R and the 18R–β_1 stages of the cycle after the 18R structure has been stabilized. This is usually rationalized considering a decrease in the free energy of the martensite, which is responsible for a shift in the equilibrium temperature between both phases. The recovery of the β_1 phase is clearly a kinetic problem, strongly related to the diffusive properties of the structures involved. An interesting example can be found in CuZnAl single crystals. It has been shown that austenitic recovery after martensitic stabilization is very fast, leading to first approaches to the problem which disregard the time intervals required for the recovery of the austenite. However, detailed experiments have shown that the recovery of the β_1 structure after stabilization of the stress induced 18R single crystal at 333 K can be well fitted by an exponential decay function with a time constant close to 900 s [39]. This time constant is approximately one order of magnitude smaller than the time constant of martensite stabilization at the same temperature (9600 s). Similar detailed results concerning the kinetics of the austenitic recovery in CuAlBe single crystals at a concentration of vacancies close to equilibrium have not been presented so far. However, results of this recovery after dynamic stabilization of martensite have shown that diffusion in CuAlBe is in fact slower than in CuZnAl. As an example, after 18R stabilization obtained by pseudoelastic cycling of CuAlBe single crystals at 353 K, the austenitic structure shows only partial recovery after 2 days at the same temperature [38], strongly suggesting that diffusion in β_1 requires higher temperatures to induce fast recovery.

Finally, it should be noticed that after retransformation from 6R into 18R, a larger sample is obtained compared with the 18R single crystal obtained by tensile stressing the austenitic structure. This behavior, which is also observed in Cu–Al–Ni [31] and in Cu–Zn–Al single crystals [19], has been attributed in the latter work to some untransformed 6R bands present in the 18R single crystal. At the moment, the same hypothesis can be made here, although *in situ* tests are to be performed to confirm this hypothesis.

4.2.5. The metastable phase transformation diagram

In the present manuscript, a metastable phase transformation diagram is presented for a single composition of the Cu–Al–Be system, with an orientation close to [100]. The temperature range has been selected in order to have the pseudoelastic effect for the austenite–18R transformation and to avoid the overlap between this transition and the formation of 6R. Metastable phase transformation diagrams have been reported for several Cu based alloys. Particularly, Cu–Zn–Al and Cu–Al–Ni alloys have been analyzed in depth [14,31,40]. Less attention has been paid to the Cu–Al–Be system, although some results have been reported concerning martensite–martensite transformations [28]. Moreover, a martensitic phase transformation diagram has been presented, which includes the formation of the 6R structure [27]. Results reported in [28] were obtained for a composition richer in Be than the one used in the present work and show the presence of three phase transformations; two of them seem to be the austenite–18R and the 18R–6R martensitic phase transitions. The third one takes place at still higher stresses and shows wide hysteresis, with about 7% deformation. Due to the higher amount of Be, the M_s of the alloys used in that paper ($M_s = 176$ K) is considerably lower than those presented here. The effects of alloy composition on the structural distortion of the 18R structure determined in [24] and introduced in the present phase transformation diagram are still unknown. However, the characteristics of the third transformation observed in [28] are completely different if hysteresis and deformation are considered, which allows us to disregard, for the moment, a correlation between both mechanisms. On the other hand, the phase transformation diagram presented in [27] corresponds to a composition quite close to the one used in the present work. We only compare the part of the diagram corresponding to temperatures higher than A_f and close to the critical temperature at which the formation of 18R and 6R martensites overlap. There are several noticeable differences, the main one being the existence of the structural distortion of the 18R structure. This distortion has interesting consequences on the shape of the phase transformation diagram. On one hand, the effect of temperature on the stress range to obtain this distortion is weaker than the Clausius–Clapeyron relationship obtained for the austenite–18R transition. This is clearly observed on the phase diagram of Fig. 4 and a consequence of this is increased deformation if test temperature is increased, together with wider hysteresis. Both features have been analyzed recently [24]. Another difference that can be noticed in the diagram presented in Fig. 4, as compared with the diagram reported in [27] and also if the comparison is extended to Cu–Zn–Al and Cu–Al–Ni alloys, is that the 6R structure does not form directly from the stress induced 18R martensite; it only forms after the 18R has distorted into 18R′. This is clearly observed in Fig. 4 for the whole temperature range analyzed. The critical stresses to form 6R show a well-defined negative slope with an extremely good correlation ($d\sigma^{18R'-6R}/dT = -0.286$ MPa/K for sample A2 in Fig. 4). A smaller absolute value was obtained for the slope $d\sigma^{6R-18R}/dT$, equal to -0.190 MPa/K in the same temperature range and for the same sample. More experimental data is required to understand the differences in the slopes obtained. However a first approach allows us to consider the average of both values as the slope corresponding to the equilibrium stress between 18R and 6R. This value enables us to estimate the entropy change between the 18R structure and the 6R martensite as 0.214 J/mol K. Concerning this point, it is interesting to consider that the entropy change between 18R and 6R is the sum of both terms $\Delta S^{18R-18R'}$ and $\Delta S^{18R'-6R}$. However, the first term can be considered negligible according to [24], which leads to the fact that the change in entropy between 18R and 6R can be reasonably estimated by the corresponding change between 18R′ and 6R. Finally, it is interesting to notice that different values of entropy change between martensitic structures have been reported both in Cu–Al–Ni and Cu–Zn–Al alloys [3,14,41]. It is reasonable to consider that the contribution to

these entropy changes should be mainly vibrational, being extremely small in some cases [14]. However, the extremely good correlation of the critical stresses presented in this manuscript indicates that an entropy change undoubtedly exists between 18R and 6R martensites and it does not depend on temperature in the temperature range considered in the present work.

5. Conclusions

- The tensile behavior of Cu–Al–Be single crystals for an axis orientation close to [100] has been studied.
- 6R martensite forms from a distorted 18R structure.
- A metastable phase transformation diagram is presented for $T > A_f$, including the structural distortion of the 18R phase.
- A good correlation has been found between the structural analysis and experimental results.
- The 18R–6R transformation in CuAlBe shape-memory alloys can be considered an interesting alternative for damping applications.

Acknowledgments

Argentina SECTyP UNCUYO – Argentina (Project 06/C387) contributed with financial support. The first author would like to express his gratitude for the doctoral fellowship provided by CONICET-Argentina.

References

[1] M. Ahlers, Prog. Mater. Sci. 30 (1986) 135–186.
[2] J.L. Pelegrina, M. Ahlers, Acta Metall. Mater. 40 (1992) 3221–3227.
[3] P. Wollants, J. Roos, L. Delaey, Prog. Mater. Sci. 37 (1993) 227–288.
[4] K. Otsuka, C.M. Wayman, in: K. Otsuka, C.M. Wayman (Eds.), Shape-Memory Materials, Cambridge University Press, Cambridge, UK, 1998, pp. 27–48.
[5] H. Warlimont, L. Delaey, Prog. Mater. Sci. 18 (1974) 59–89.
[6] K. Otsuka, T. Ohba, Proceedings of ICOMAT 1992, Monterey, CA, USA, 1992, pp. 221–232.
[7] R. Rapacioli, M. Ahlers, Acta Metall. 27 (1979) 777–784.
[8] L. Mañosa, M. Jurado, A. González-Comas, E. Obradó, A. Planes, J. Zarestky, C. Stassis, R. Romero, A. Somoza, M. Morin, Acta Mater. 46 (1998) 1045–1053.
[9] F. Lanzini, R. Romero, M.L. Castro, Intermetallics 16 (2008) 1090–1094.
[10] V. Recarte, R.B. Pérez-Saez, E.H. Bocanegra, M.L Nó, J. San Juan, Metall. Mater. Trans. A 33 (2002) 2581–2591.
[11] K. Otsuka, H. Sakamoto, K. Shimizu, Acta Metall. 27 (1979) 585–601.
[12] P. Arneodo, A.M. Condó, M. Ahlers, Philos. Mag. 85 (2005) 2491–2525.
[13] J.L. Pelegrina, M. Ahlers, Acta Metall. Mater. 40 (1992) 3205–3211.
[14] M. Ahlers, J.L. Pelegrina, Acta Metall. Mater. 40 (1992) 3213–3220.
[15] G. Barceló, M. Ahlers, R. Rapacioli, Z. Metallkd. 70 (1979) 732–738.
[16] K. Takezawa, T. Izumi, H. Chiba, S. Sato, J. Phys. C4-43 (1982) 819–824.
[17] Z. Saburi, Y. Inada, S. Nenno, N. Hori, J. Phys. C4-43 (1982) 633–638.
[18] H. Sakamoto, Y. Nakai, K. Shimizu, Trans. JIM 28 (1987) 765–772.
[19] F. de Castro Bubani, M. Sade, F.C. Lovey, Mat. Sci. Eng. A 543 (2012) 88–95.
[20] A. Cuniberti, R. Romero, Mater. Sci. Eng. A 273–275 (1999) 362–365.
[21] N. Siredey, A. Eberhardt, Mater. Sci. Eng. A 290 (2000) 171–179.
[22] A. Tidu, A. Eberhardt, B. Bolle, F. Moreau, J.J. Heizmann, J. Appl. Crystallogr. 34 (2001) 722–729.
[23] C.H. González, C.J. De Araújo, N.F. Quadros, G. Guénin, M. Morin, Mater. Sci. Eng. A 378 (2004) 253–256.
[24] M. Sade, A. Yawny, F.C. Lovey, V. Torra, Mater. Sci. Eng. A 528 (2011) 7871–7877.
[25] J. Oldbricht, A. Yawny, J.L. Pelegrina, A. Dlouhy, G. Eggeler, Metall. Mater. Trans. A 42A (2011) 2556–2574.
[26] F. Saule, M. Ahlers, Acta Metall. Mater. 43 (1995) 2373–2384.
[27] A. Hautcoeur, A. Eberhardt, E. Patoor, M. Berveiller, J. Phys. C2-5 (1995) 459–464.
[28] R. Amireche, M. Morin, Proceedings of ICOMAT 2008, Santa Fe, 2008, pp. 577–580.
[29] J. Van Humbeeck, L. Delaey, in: E. Hornbogen, N. Jost (Eds.), The Martensitic Transformation in Science and Technology, DGM, Oberursel, 1989, pp. 15–25.
[30] M. Sade, R. Rapacioli, F.C. Lovey, M. Ahlers, J. Phys. C4-43 (1982) 647–652.
[31] K. Otsuka, H. Sakamoto, K. Shimizu, Acta Metall. 27 (1978) 585–601.
[32] F.C. Lovey, Acta Metall. 35 (1987) 1103–1108.
[33] F. Saule, A. Tolley, M. Ahlers, Scr. Metall. Mater. 24 (1990) 363–368.
[34] J. De Vos, E. Aernoudt, L. Delay, Z. Metallkd. 69 (1978) 438–444.
[35] A. Kelly, G.W. Groves, Crystallography and Crystal Defects, Longman, London169–191.
[36] F. De Castro Bubani, M. Sade, F.C. Lovey, Mater. Sci. Eng. A 577 (2013) 147–157.
[37] S. Kustov, J. Pons, E. Cesari, M. Morin, Scr. Mater. 46 (2002) 817–822.
[38] M. Sade, F.C. Lovey, V. Torra, A. Yawny, Proceedings of ESOMAT 2009 06036 (2009), Prague, Czech Republic, 2009. http://dx.doi.org/10.1051/esomat/200906036.
[39] A. Yawny, F.C. Lovey, M. Sade, Mater. Sci. Eng. A 290 (2000) 108–121.
[40] J.L. Pelegrina, M. Ahlers, Acta Metall. Mater. 38 (1990) 293–299.
[41] K. Otsuka, K. Shimizu, Proceedings of ICOMAT 1979, Cambridge, MA, USA, 1979, pp. 607–618.